Intraseasonal Oscillation of Convective Activity in the Tropical Southern Hemisphere: May 1984–April 1986

DAYTON G. VINCENT

Department of Earth and Atmospheric Sciences, Purdue University, West Lafayette, Indiana

THOMAS SPERLING, ANDREAS FINK, STEFAN ZUBE AND PETER SPETH

Institut fur Geophysik u. Meteorologie, Universitat zu Koln, Koln, Federal Republic of Germany

(Manuscript received 8 March 1990, in final form 6 August 1990)

ABSTRACT

The intraseasonal (40–50 day) oscillation in convection over the tropical Southern Hemisphere (0°–15°S) is examined using two years of ECMWF analyses. The initial period investigated was 1 May 1984–30 April 1986. This diagnosis revealed that the oscillation was essentially absent in the Southern Hemisphere during the winter months. Therefore, the paper focuses on two subperiods, 1 November 1984–30 April 1985 (Year 1) and 1 September 1985–15 April 1986 (Year 2), when the oscillation could be detected. Although several variables were examined, the velocity potential at 200 hPa (χ_2) and outgoing longwave radiation (OLR) were found to be the best indicators of the oscillatory convective activity; consequently, these variables are the only ones presented. One of the unique features of this study is that the data were not temporally filtered, except for removing the time mean and linear trend, until after it was established that statistically significant peaks occurred on the intraseasonal time scale. This was an important step in this case because the dominant spectral peaks for the oscillation in each year were considerably different. In Year 1 the significant intraseasonal period was between 50 and 67 days, while in Year 2 it was centered near 33 days. Based on this, a recursive bandpass filter of 40–80 days was applied to Year 1 and 27–44 days to Year 2. If the data was temporally filtered at the onset (e.g., 30–60 day band pass), the proper conclusions may not have been reached.

For the most part, the findings agree with those of previous investigators. The oscillation propagated eastward, and its convective activity in both years was more intense over the Indian Ocean–Indonesia–western Pacific region than elsewhere. Furthermore, the χ_2-wave could be followed continually around the globe, but the convection (OLR) associated with the oscillation was weak and difficult to track over much of the Western Hemisphere. The primary difference between the two years, besides the period of oscillation, was that the correlation between χ_2 and OLR was much greater in Year 1.

1. Introduction

As is well known, deep convection in the tropics undergoes changes on several temporal scales (e.g., Webster 1983). A seasonal variation takes place as the intertropical convergence zone (ITCZ) meanders north and south across the equator. The occurrence of enhanced convective activity associated with the Australian summer monsoon is an excellent example on this time scale. There is also an interannual variation, the best example of which is the increased convection in the vicinity of warm sea surface temperature anomalies associated with an El Niño/Southern Oscillation (ENSO) event. Of interest in the present study, however, are the intraseasonal variations, or modulations, that take place in the convection within the Southern Hemisphere tropics. A prime example on this time scale, and the one that represents the focus of the present paper, is the Madden and Julian (1971, 1972) "40–50 day" oscillation that occurs in the convection and its corresponding circulation features.

Numerous investigators have examined the 40–50 day oscillation (e.g., Krishnamurti et al. 1985; Lau and Chan 1985; Weickmann et al. 1985; Knutson et al. 1986; Madden 1986; Knutson and Weickmann 1987; von Storch et al. 1988; and Gutzler and Madden 1989). A consensus of their opinions suggests that the oscillation generally has the following properties and characteristics. It:

1) consists primarily of an eastward propagating, wavenumber one, Kelvin wave with an average speed of 10 m s^{-1};
2) has a variable period from approximately 25 to 75 days;
3) has its strongest amplitude and slowest propagation speed ($\sim$5 m s^{-1}) from about 60°E to 180°;
4) sometimes difficult to identify east of the date

Corresponding author address: Dr. Dayton G. Vincent, Dept. of Earth & Atmos. Sciences, Civil Engineering Bldg., Purdue University, West Lafayette, IN 47907.

line because the convection often becomes weaker over the eastern Pacific;

5) frequently exists in a dipole fashion in the zonal plane (i.e., Walker Circulation) in which the Indian Ocean–Indonesian region (60°–120°E) is out of phase with the central Pacific–SPCZ region (i.e., when one region has strong convection, the other has weak convection);

6) is predicted by models to have one-half the periodicity (twice the phase speed) of that which is observed; and

7) can sometimes be detected as far as 20°–30° from the equator.

Many prior investigations of the oscillation have studied and detected its existence through the use of data-filtering techniques (e.g., bandpass) or empirical orthogonal functions, and less attention has been devoted to determining if a statistically significant signal is associated with the oscillation. A unique aspect of the present investigation is that the "unfiltered" data are examined first, with only the time mean and linear trend removed. Statistical analyses, described in section 2, are performed in order to detect the significant peaks in the spectral distribution. The appropriate time filtering is then performed for further diagnosis. Two years of data are examined and, had the data been temporally filtered first, it is possible that the amplitude of the oscillation would have been dampened considerably, or even missed in one or perhaps both years (section 3). Furthermore, the approach used here provides assurance that the oscillations detected represent an important component of the total flow.

The period of this investigation is from May 1984 to April 1986. This period was selected because it is not affected by an ENSO episode. The data sources used are the global operational analyses from the European Centre for Medium-range Weather Forecasts (ECMWF) and the standard NOAA dataset of outgoing longwave radiation (OLR). Further discussion of data sources, data processing, computational procedures, and statistical methods is given in the next section. Results and discussion are presented in section 3 and a summary is given in section 4.

2. Data sources and computational methods

The ECMWF analyses used here were provided in spherical harmonics, with a triangular truncation of T63, but these data were transformed to 3° latitude by 5° longitude grid. The analyses were available at 00 UTC each day at standard pressure levels up to 30 hPa and contained geopotential height, temperature, relative vorticity, horizontal divergence, vertical velocity, and relative humidity. Horizontal wind components were computed from vorticity and divergence, and velocity potential from divergence. Since the analyses were global, no boundary conditions were required for the computation of velocity potential. The OLR data were provided at increments of 2.5° latitude by 2.5° longitude and are essentially the values described by Gruber et al. (1986). The dataset contains daily values, but 5-day running means were calculated to overcome the problem of missing data at some longitudes.

Since spectral analysis forms a major part of the statistical methods used in this paper, the techniques applied to compute various power spectra are now presented. A stochastic process is simply described by its autocovariance function. An equivalent description is provided by its power spectrum, which is the Fourier transform of the autocovariance function. The power spectrum curve shows how the variance of the stochastic process is distributed with respect to frequency.

The procedure applied is based on the lag method and is described by Jenkins and Watts (1968). A discrete stochastic time series is designed for some variable, x, by

$$x_i = x(t_i), \quad i = 1, \quad n < \infty$$

where

$$t_{i+1} - t_i = \Delta t = \text{const.}$$

Then, the time mean and linear trend were removed from the time series of x and the time series was correlated with itself by applying a time lag about a specified number of time steps, $k\Delta t$. From this, an autocovariance function, $c_{xx}(k)$, was obtained

$$c_{xx}(k) = \frac{1}{n} \sum_{i=1}^{n-k} (x_i - \bar{x})(x_{i+k} - \bar{x}), \quad k = 0, \quad m < n$$

where $\bar{x}$ is the arithmetic average and m is the maximum possible lag. The value of c_{xx} was computed for all time lags, k, where $|k| \leqslant m$; for $|k| > m$, c_{xx} is not defined.

In order to apply a Fourier transform, assumptions must be made concerning the behavior of c_{xx} outside the interval, $[0, m]$. Thus, a new autocovariance function, $u_{xx}(k)$, is defined as:

$$u_{xx}(k) = c_{xx}(k)w(k)$$

where

$$w(k) = \begin{cases} \frac{1}{2}\left(1 + \cos\frac{\pi k}{m}\right), & |k| \leqslant m \\ 0, & k > m \end{cases}$$

is a weighting function.

The final Fourier transform can now be written as

$$C_{xx}(f) = 2\left(u_{xx}(0) + 2\sum_{k-1}^{m-1} u_{xx}(k)\cos\frac{\pi k f}{m}\right), \quad 0 \leqslant f \leqslant m.$$

To obtain a correlation between two variables, x and y, one can derive a cross spectrum, C_{xy}, with the time

series, x_i, y_i. The procedure is the same as for C_{xx}. This technique is applied and the coherency of the time series, x_i, y_i, is obtained using

$$K_{xy}^2(f) = \frac{L_{xy}^2(f) + Q_{xy}^2(f)}{C_{xx}(f) \cdot C_{yy}(f)}$$

where $L_{xy}(f)$ and $Q_{xy}(f)$ are the co- and quadrature spectra, respectively.

Due to the finite length of our time series, the spectral values could only be estimated. Therefore, the 95% confidence interval was computed for each variable. This interval is used, relative to the red noise, to determine significant periods in the spectral distribution. After finding the particular period of interest (i.e., the dominant intraseasonal oscillation), the behavior of this oscillation was investigated by applying the appropriate bandpass filter. To do so, this oscillation was separated from modes of other time scales in the original time series. This was accomplished by using the recursive filter technique described by Murakami (1979). As before, the time mean and linear trend were removed from the data. Then, values of ω_0, ω_1 and ω_2 (measured by 2π/period) were determined, where ω_0 denotes a 100% response, and ω_1 and ω_2 correspond to a 50% response on each side of ω_0. As noted by Murakami, only one of the latter two must be determined, because the following relationship has to be satisfied:

$$\omega_0^2 = \omega_1 \omega_2.$$

The advantage of applying this technique is that it converged so rapidly there was no need for concern with the cutoff problem, which can arise in a relatively short time series if a numerical bandpass filter with weighted values is used.

3. Results and discussion

Although the primary interest of this research was to investigate the intraseasonal oscillation of deep convection over the Southern Hemisphere tropics, the convective activity over the equatorial belt, 9°N–9°S, was first examined. This was done in order to see what evidence there was to support the year-round existence of the oscillation since there is some disagreement in the literature concerning this point (e.g., Murakami et al. 1983; Lorenc 1984; Krishnamurti et al. 1985; Weickmann et al. 1985). Here the analyses (not shown) included time series over the two-year period of study of several variables at discrete grid points, stretching from the central Indian Ocean to the eastern Pacific Ocean. A map of this sector of the globe is provided in Fig. 1. The variables examined were the zonal wind component at 200 and 850 hPa, horizontal divergence and velocity potential at 200 hPa, temperature at 500 hPa, and OLR. Of these, the velocity potential (χ_2) and OLR yielded the best signal of the oscillation. These variables also appeared to behave in a more periodic manner, with respect to the oscillation, and produced a stronger indication of convection in the southern summer months. Perhaps the reason for this was the domination and interference of the Asian monsoon circulation during northern summer. At any rate, since our primary interest was in the tropical Southern Hemisphere, attention was focused on the southern summer period and further studies were conducted using χ_2 and OLR.

Figure 2 shows a sample of some of the time series of χ_2 that were examined over the two-year period for the Southern Hemisphere tropical belt, 0°–15°S. Area averages were computed for all longitude bands, each 15° in width, from 60°E to 120°W; only three longitudinal bands are shown in Fig. 2 to conserve space.

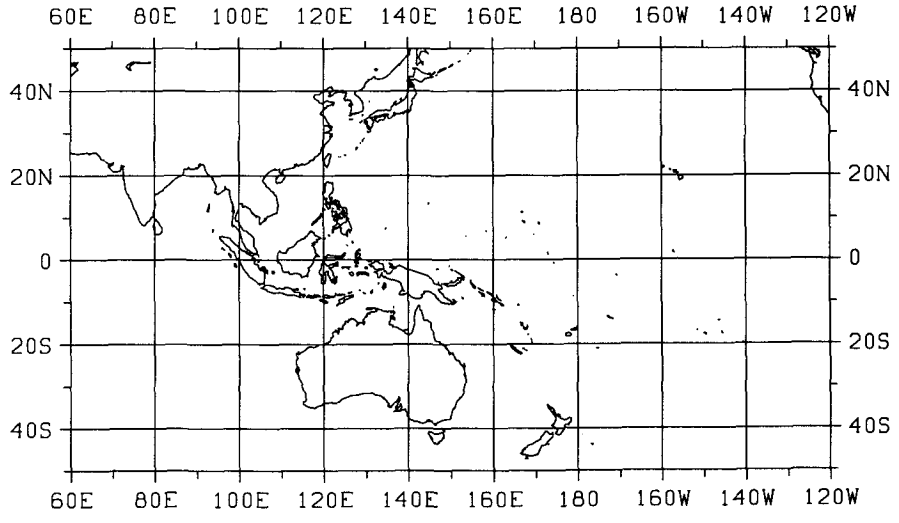

FIG. 1. Map showing primary area of interest.

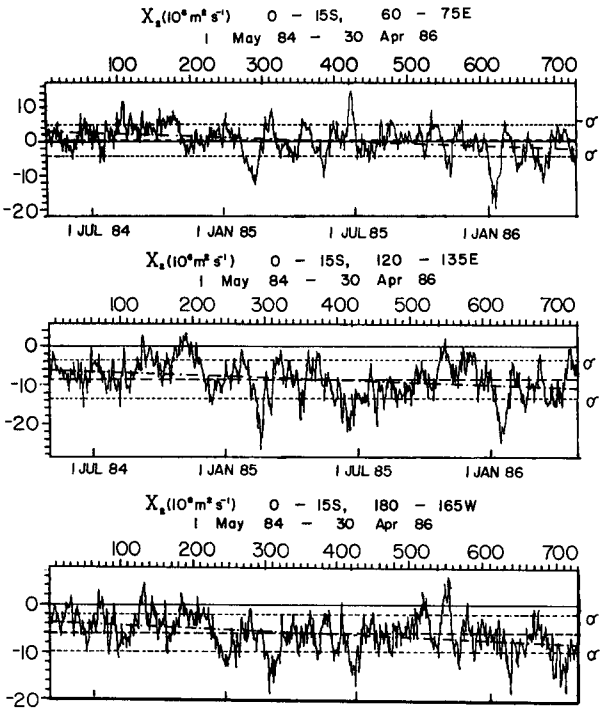

FIG. 2. Time series of velocity potential at 200 hPa, χ_2 (10^6 m^2 s^{-1}) for 1 May 1984–30 April 1986, averaged from 0° to 15°S and from (a) 60° to 75°E, upper panel, (b) 120° to 135°E, middle panel, and (c) 180° to 165°W, lower panel. Also shown are the mean (dashed), ± one standard deviation, σ (dotted), and the trend (dot-dash).

Some points are worth noting in this figure. First, the largest negative values (minima) are seen to occur in February 1985 (~ Days 290–300) and January 1986 (~ Days 620–630). Second, during each of these periods an eastward propagation of the minimum value is indicated. When we examined all longitude bands, a quasi-periodic eastward propagation of both minima was found, which is characteristic of the 40–50 day oscillation. More will be said and illustrated later concerning this point. Third, evidence of the oscillation during the winter months, June–July–August, is not as obvious as it is during most of the remaining months. This agrees with the finding of Murakami et al. (1986) who state that the oscillation tends to be strongest in the Summer Hemisphere. Fourth, there is an identifiable linear trend evident within each longitude band. We suspect this is due, at least in part, to changes made in the ECMWF analysis–forecast system on 1 May 1985, which probably caused an increase in upper tropospheric divergence in the tropics (Trenberth and Olson 1988). However, this appears to have little effect on the purpose of the present paper.

The energy spectrum response of the amplitude of χ_2 (not shown) yielded a relatively strong signal near 65 days at all three longitude bands in Fig. 2 (as well as others); however, the signal was not *statistically significant* at the 95% confidence interval. Since the plots of χ_2 appear to exhibit a more periodic behavior, with respect to the oscillation, during the summer months, the winter periods were excluded from the study to see if the signal of the oscillation would become *statistically significant.* Consequently, subsequent illustrations and discussion focus on the following periods, November 1984–April 1985 (Year 1) and September 1985–April 1986 (Year 2), which were found to contain the best representations of the intraseasonal oscillation.

a. Year 1

Figure 3 shows a sample of the time series of χ_2 and OLR (with the time mean and linear trend removed) at selected longitude bands for the Year 1, 6-month period. It should be noted that no consistently identifiable trend was observed in either variable for this period. Also shown in Fig. 3 are the energy spectra from the frequency response for each variable. As was the case for the time plots in Fig. 2, those in Fig. 3 were computed for areas that were 15° longitude in width and bounded by latitudes, 0° and 15°S, for the region from 60°E to 120°W. To conserve space, only a representative number of longitudinal bands are illustrated. A view of the energy spectra results for the longitude band, 90°–105°E (Fig. 3a) reveals that both χ_2 and OLR had a statistically significant peak at the 95% confidence interval near the 67-day period (actually 66.7 days). Similar results were obtained for other bands across the Indian Ocean. The same peak is still detectable in both variables over Indonesia (120°–135°E), but it was not strong enough to be statistically significant at the 95% interval (Fig. 3b). Figure 3c shows that this peak remains important over the western Pacific (165°E–180°) and is again statistically significant for OLR. East of the date line (165°–150°W), the 67-day period continues to show a peak in the χ_2 spectra; however, that peak has vanished in the OLR spectra (Fig. 3d). It should be noted that, within the intraseasonal time frame, many of the time series in Fig. 3 also show a significant peak, or at least indicate a strong response, near 50 days.

The time series of χ_2 and OLR suggest that the two variables are well correlated over the Indian Ocean–Indonesia–western Pacific region (Figs. 3a–c), but are not as well correlated to the east of the date line (Fig. 3d). Furthermore, in the region west of the date line where the time series of χ_2 and OLR are very similar, three points are worth noting: 1) there is an eastward progression of the maxima and minima of both variables; 2) the period of their apparent oscillation is between 50 and 67 days; and 3) the period of largest negative values of χ_2 occurs in February 1985, as noted previously in Fig. 2. The values of the cross-spectral coefficient between χ_2 and OLR are given in Table 1 for all longitude bands using a period of 66.7 days. They lend support to our interpretation of the results

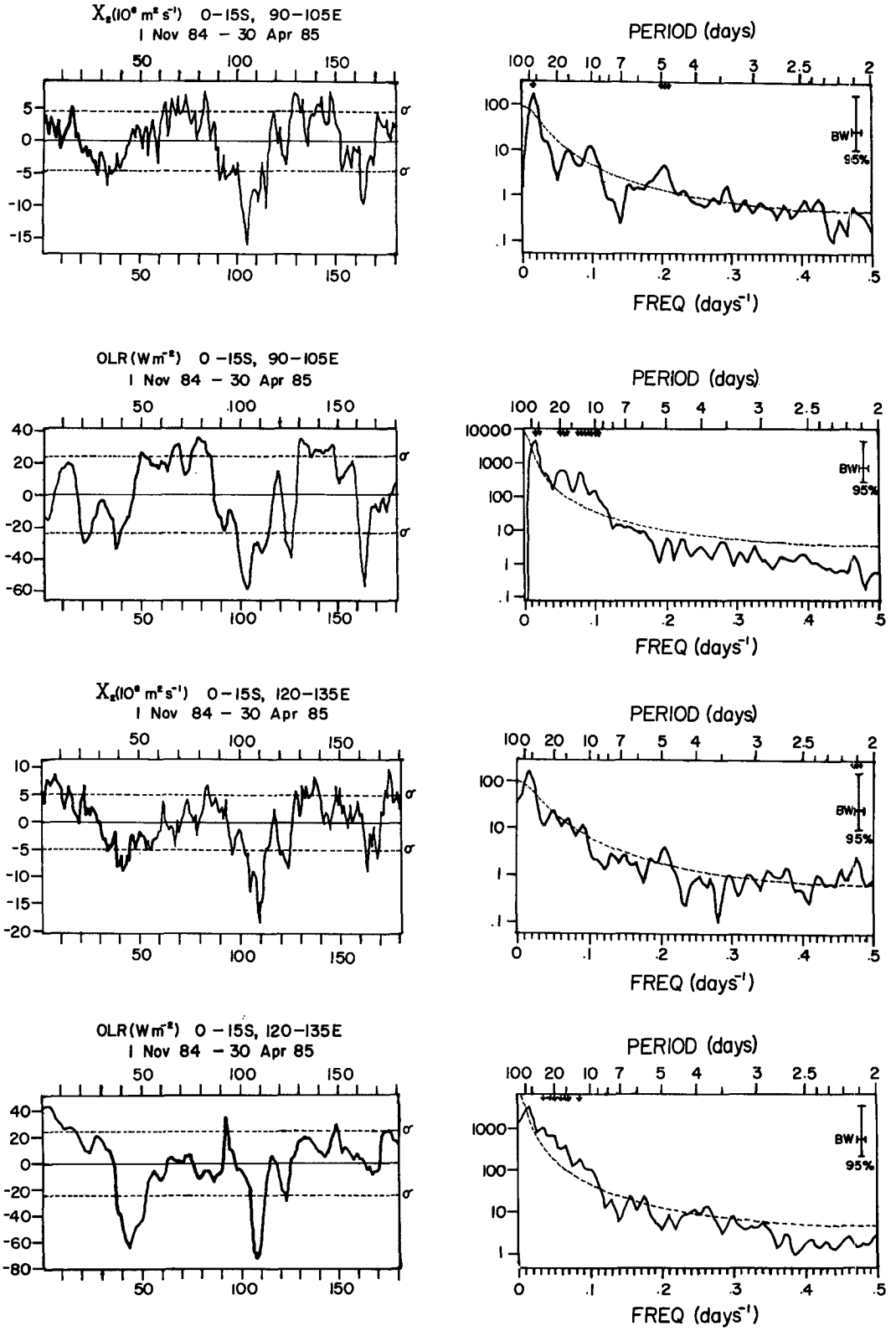

FIG. 3. Time series of χ_2 (10^6 m^2 s^{-1}) and 5-day running mean OLR (W m^{-2}) for 1 November 1984–30 April 1985 with mean and linear trend removed and $\pm 1\ \sigma$ given (dotted). Also shown are the amplitudes for each variable in the form of energy (power) spectra with arrows indicating periods $\geq$ 95% confidence interval. All values were averaged from 0° to 15°S and from (a) 90° to 105°E, (b) 120° to 135°E, (c) 165°E to 180°, and (d) 165° to 150°W.

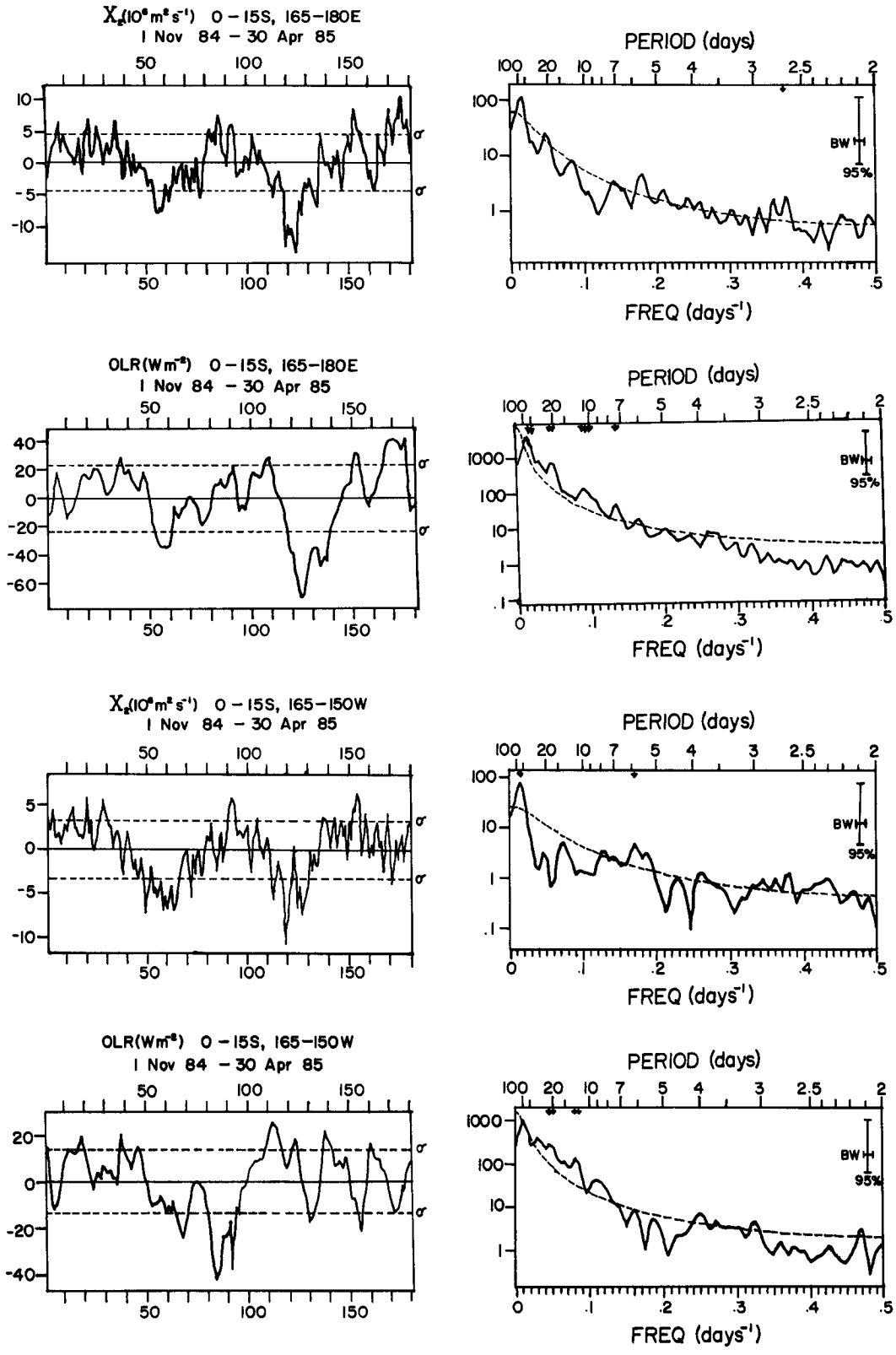

FIG. 3. (*Continued*)

TABLE 1. Cross-correlation coefficients (χ_2, OLR) averaged from 0°–15°S for 66.7 day period between 1 November 1984 and 30 April 1985.

Longitudes	Coefficients
60°–75°E	0.95
75°–90°E	0.94
90°–105°E	0.94
105°–120°E	0.91
120°–135°E	0.91
135°–150°E	0.74
150°–165°E	0.76
165°–180°E	0.91
180°–165°W	0.91
165°–150°W	0.59
150°–135°W	0.68
135°–120°W	0.79

shown in Fig. 3. Similar results (not shown) were found for the cross-spectral coefficients when a period of 50 days was used.

The results shown thus far infer that the intraseasonal signal of the convection (as indicated by the OLR) decreases relative to that of the upper level circulation (as indicated by χ_2) when the oscillation reaches the central Pacific. This finding is not unique to the present investigation, as mentioned in the consensus description of the characteristics of the oscillation in section 1. Furthermore, as with most previous investigations, it was found that the χ_2 oscillation could be followed across the eastern Pacific and, as will be shown later, around the globe. Nonetheless, the main point emphasized here is that the characteristics and properties of the oscillation are generally statistically significant and were obtained without any temporal filtering of the data, except for trend removal.

For detecting the spatial distribution of the oscillation, a Hovmoeller diagram of χ_2 (with the time mean and linear trend removed) is presented for the 6-month period in Year 1, 1 November 1984–30 April 1985 (Fig. 4). As for the previous diagrams, values have been averaged over the latitude belt, 0°–15°S. For convenience, values of $\chi_2 \leq -4$ units are shaded to illustrate where and when the largest negative anomalies occurred. The quasi-periodic nature of the circulation is clearly visible in Fig. 4 and indicates that a wave of maximum negative values propagates around the globe, essentially uninterrupted, approximately three times during the 6-month period. The average period of the wave appears to lie somewhere between 50 and 67 days, which is in agreement with the statistical results shown earlier. This period yields an average phase speed of about 8 m s^{-1}, but the wave appears to propagate at a slower speed in the eastern hemisphere than in the western hemisphere. These characteristics of the wave also correspond favorably to the consensus of properties stated in section 1.

Now since it has been established that the signal of

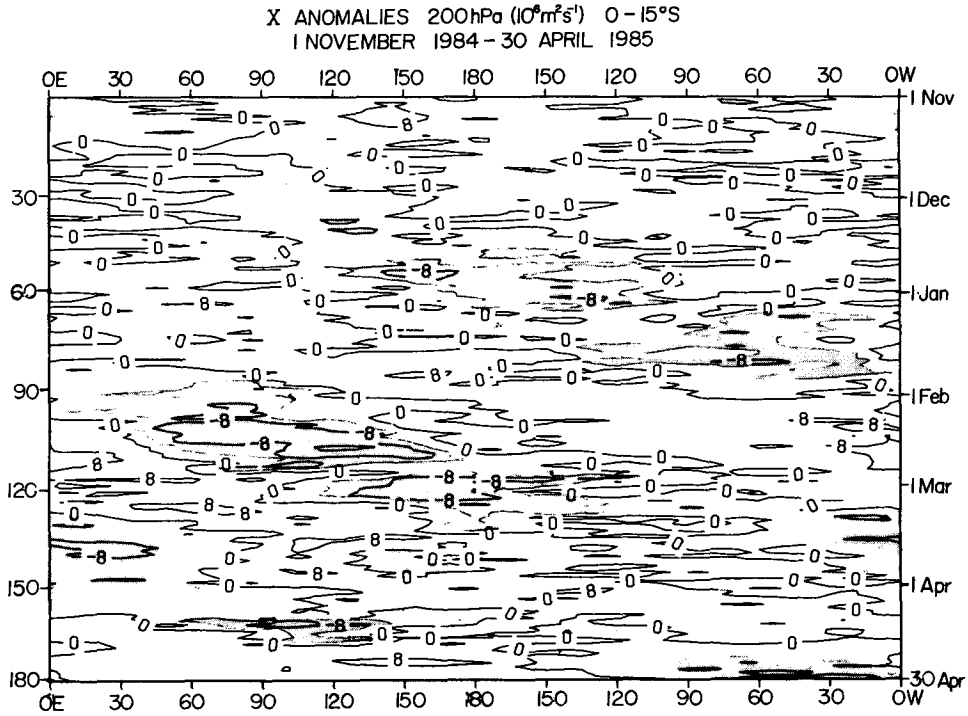

FIG. 4. Hovmoeller diagram of χ_2 for 1 November 1984–30 April 1985 with mean and linear trend removed, averaged from 0° to 15°S. Values $\leq -4 \times 10^6$ m^2 s^{-1} are shaded and contour interval is 4.

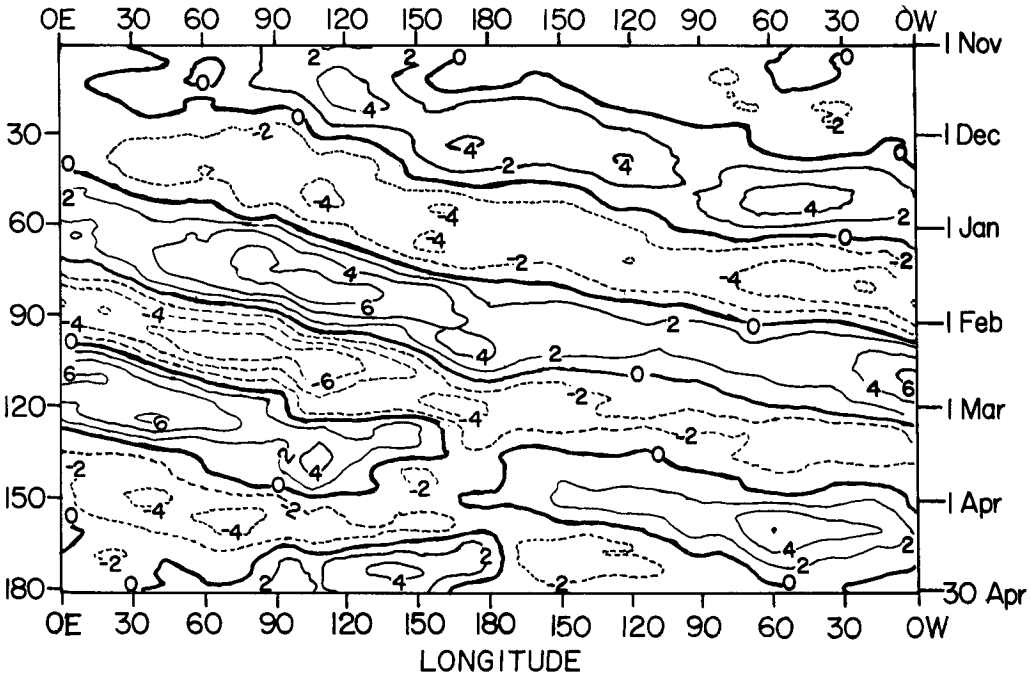

FIG. 5. Hovmoeller diagram of the recursive bandpass 40–80 day filter applied to the χ_2 distribution shown in Fig. 4 (see text for details). Dashed lines depict negative values and contour interval is 2.

the intraseasonal oscillation is statistically significant and that the wave travels eastward in a nearly continuous manner with a period of 50–67 days, it is with confidence that a bandpass filter is applied to χ_2. Figure 5 shows the result of applying the recursive bandpass filter, described in section 2, to χ_2 for Year 1. The values

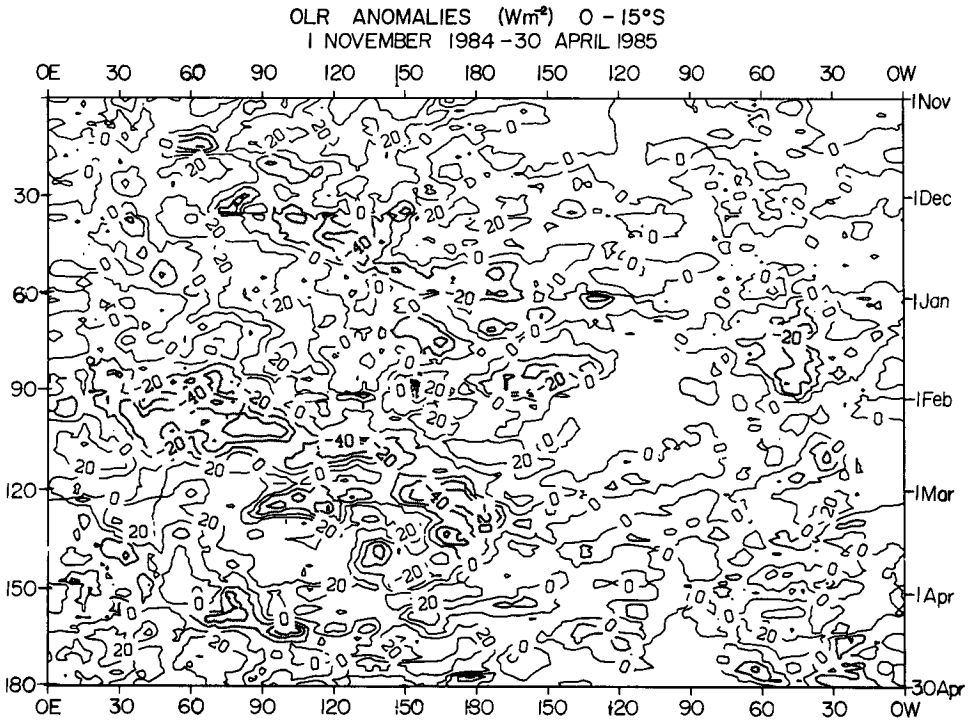

FIG. 6. As in Fig. 4, except for 5-day running mean OLR with values ≤ -20 W m^{-2} shaded. Contour interval is 20.

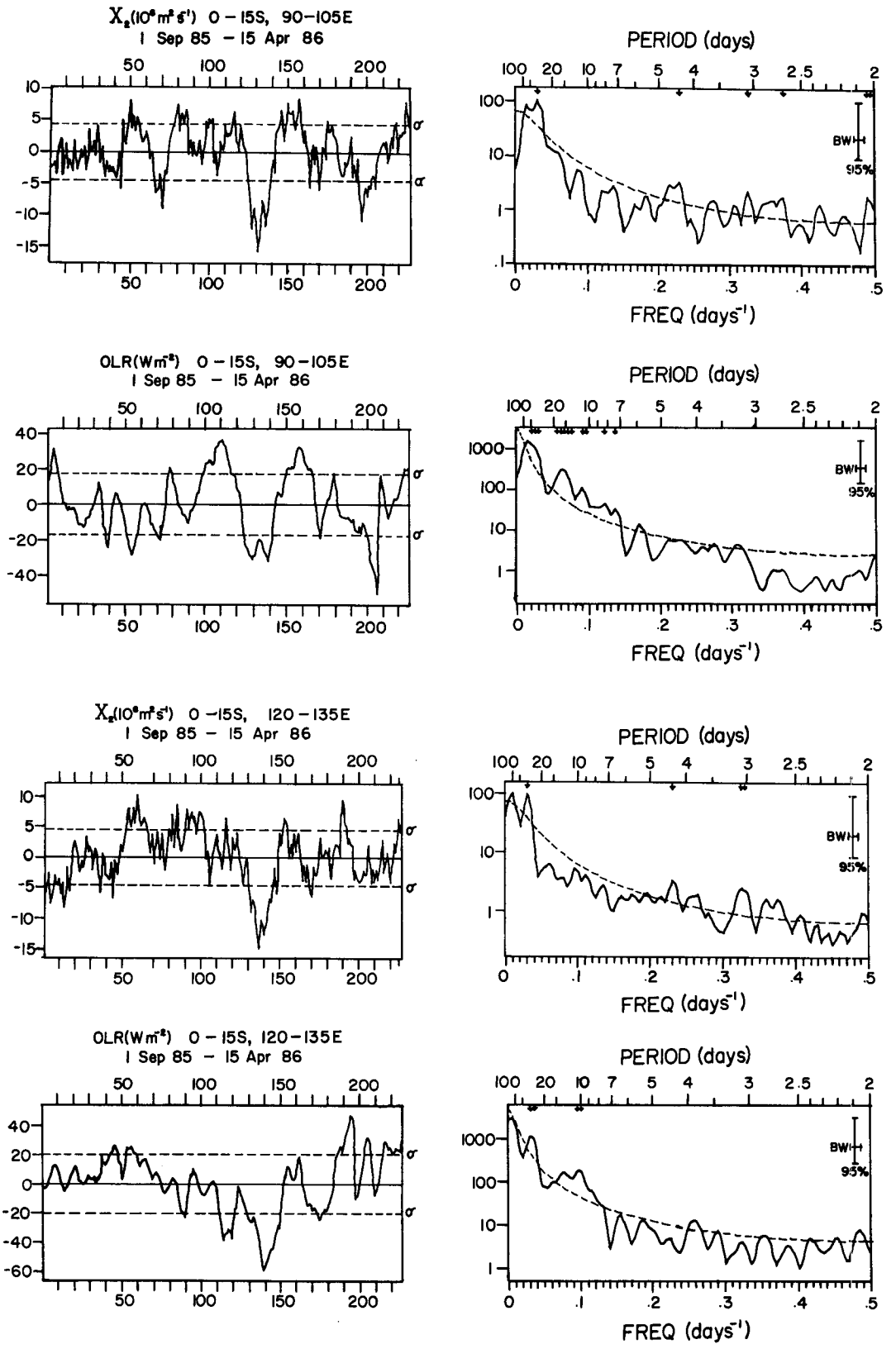

FIG. 7. As in Fig. 3, except for 1 September 1985–15 April 1986.

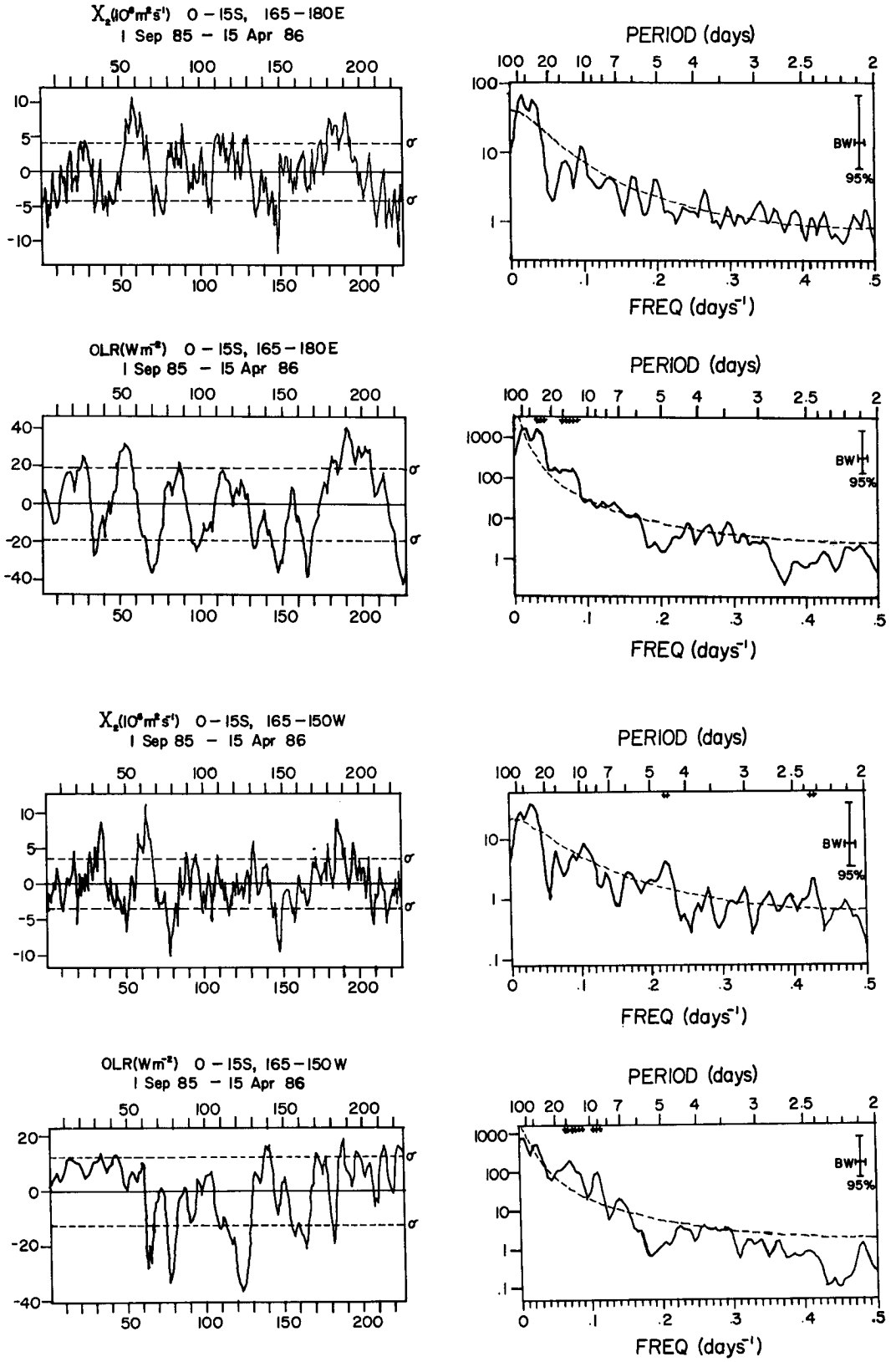

FIG. 7. (*Continued*)

of ω_0, ω_1, and ω_2 were 57, 40, and 80 days, respectively. It is seen that the propagation pattern of Fig. 5 is in good agreement with that in Fig. 4, verifying that the bandpass filter selected captured the correct phase angle of the oscillation. It is seen that the filtered portion of χ_2 is a main contributor to the total flow.

A Hovmoeller diagram of the OLR averaged from 0°–15°S, with time mean and linear trend removed, is presented in Fig. 6. Two points are worth noting. First, the OLR anomalies are greatest over the region stretching from the Indian Ocean to the central Pacific. Second, there is a good correspondence between the largest negative anomalies of OLR and χ_2 (compare Figs. 4 and 6.) Thus, as suggested by the results of Fig. 3 and as found by other investigators, the correlation between the convection and upper-level circulation is strongest in the eastern hemisphere. It should be noted that the pattern of OLR anomalies in Fig. 6 is in excellent agreement with a similar pattern for 10°N–10°S, as discussed by Weickmann (1985).

b. Year 2

The same statistical tests were run for Year 2 as for Year 1 and the same diagrams were constructed, except that the total period examined in Year 2 was 7½ months instead of 6 months. The examination of Year 2 was started two months earlier than Year 1 because the time series of χ_2 in Fig. 2 indicated that an intraseasonal oscillation in the Southern Hemisphere might be present as early as September 1985. The Hovmoeller diagrams of χ-anomalies at 250 hPa, averaged from 20°N–20°S, which appear in the February 1986 issue of the *Climate Diagnostics Bulletin* and are discussed by Weickmann (1986), also suggest a signal of the oscillation as early as September. For figures involving OLR, Year 2 was ended on 15 April 1986 because of excessive missing data. The time series of χ_2 and OLR, together with their energy spectra, are shown in Fig. 7 for the same four longitudinal bands as for Year 1 (Fig. 3). Also, as for Year 1, variables were averaged from 0°–15°S. The major difference between the results of the two years is that Year 2 shows a preferred response for the amplitude of the oscillation to be about 30–35 days (actually 33 days), whereas Year 1 showed approximately twice that period. As for Year 1 findings, Year 2 results were in excellent agreement with those of Weickmann (1986). Two other points are worth mentioning before discussing the details of Fig. 7. First, the time series of χ_2 and OLR are not as well correlated in Year 2 as in Year 1; second, for most of the longitude bands, a downward trend was evident in Year 2, whereas no trend occurred in Year 1. The reason for the downward trend during the second year is probably because the time series was started in September (see Fig. 2).

Figure 7a illustrates the time series (with time mean and linear trend removed) and energy spectra of χ_2 and OLR for the longitude band, 90°–105°E. It shows the largest negative anomalies to be centered near Day 130, which is in early January 1986. This was noted earlier with respect to the original time series in Fig. 2. The plot of OLR indicates that a maximum in convective activity occurred in conjunction with this minimum of χ_2. The correspondence between χ_2 and OLR elsewhere is not so obvious. The energy spectra of χ_2 in Fig. 7a show a statistically significant peak at the 95% confidence interval near 33 days, as does the OLR. However, the OLR spectra have significant peaks at several other periods; therefore, the cross-correlation coefficient at 33 days is not very high (see Table 2). The results shown in Fig. 7a are typical of the Indian Ocean region (60°–120°E), with the possible exception of the 75°–90°E band (Table 2).

In contrast, the correlation between χ_2 and OLR is considerably better over Indonesia and the western Pacific. The energy spectra in Fig. 7b (120°–135°E) show a statistically significant peak for both variables near the 33-day period, and Fig. 7c (165°E–180°) shows a strong response for the same period, although not quite significant at the 95% interval for χ_2. Except for the band, 135°–150°E, Table 2 verifies that the correlation between χ_2 and OLR is good from 120°E to the date line. The time series in Fig. 7b,c also show the continued eastward movement of the strong negative anomaly in January 1986. As with Year 1, however, it appears that the OLR signal associated with the intraseasonal oscillation weakens considerably as the wave propagates over the central and eastern Pacific Ocean (Fig. 7d). The time series and energy spectra of χ_2 indicate that an eastward-traveling wave with a period of about 33 days is still present from 165°–150°W, but the OLR data do not. Furthermore, the cross-correlation coefficients between the two variables are quite low east of the date line (Table 2).

A Hovmoeller diagram of χ_2, with the time mean and linear trend removed, is shown in Fig. 8. In contrast to Fig. 7, the ending date for this diagram is 30 April 1986. An eastward-propagating wave with a period of

TABLE 2. Cross-correlation coefficients (χ_2, OLR) averaged from 0°–15°S for 33.3 day period between 1 September 1985 and 15 April 1986.

Longitudes	Coefficients
60°–75°E	0.36
75°–90°E	0.66
90°–105°E	0.31
105°–120°E	0.11
120°–135°E	0.61
135°–150°E	0.35
150°–165°E	0.67
165°–180°E	0.85
180°–165°W	0.32
165°–150°W	0.16
150°–135°W	0.56

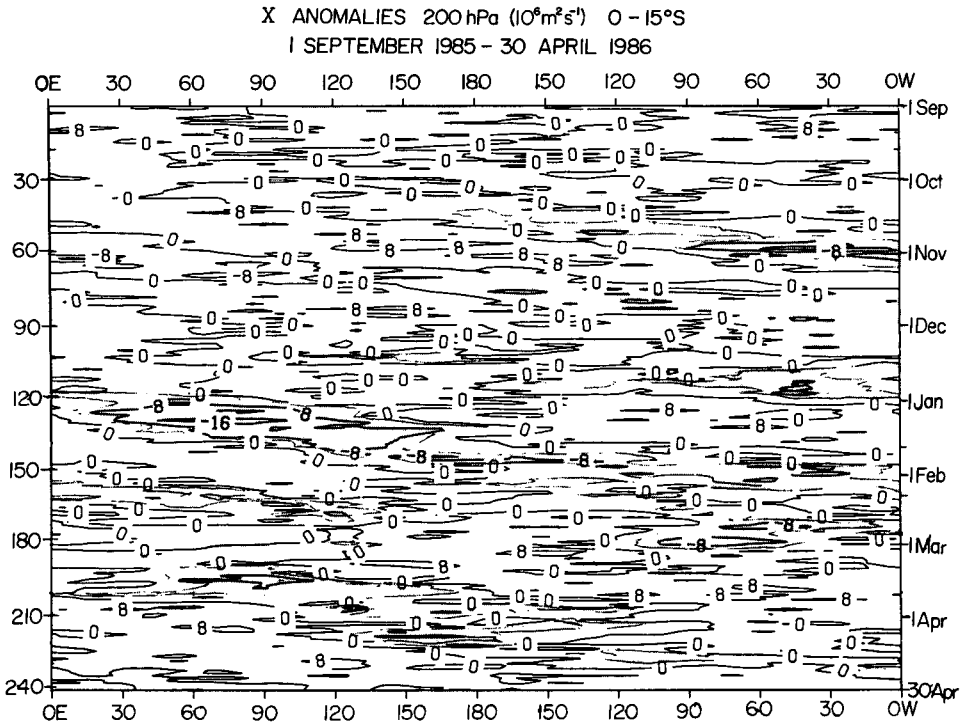

FIG. 8. As in Fig. 4, except for 1 September 1985–30 April 1986.

approximately 33 days is evident. Throughout most of the 8-month period it is possible to follow the wave around the globe. There is also a tendency, particularly over the eastern hemisphere and central Pacific, for all waves with a period between 30 to 70 days to exhibit larger negative values. This tendency can also be seen in the energy spectra of χ_2, which frequently showed a strong, but not statistically significant, response near

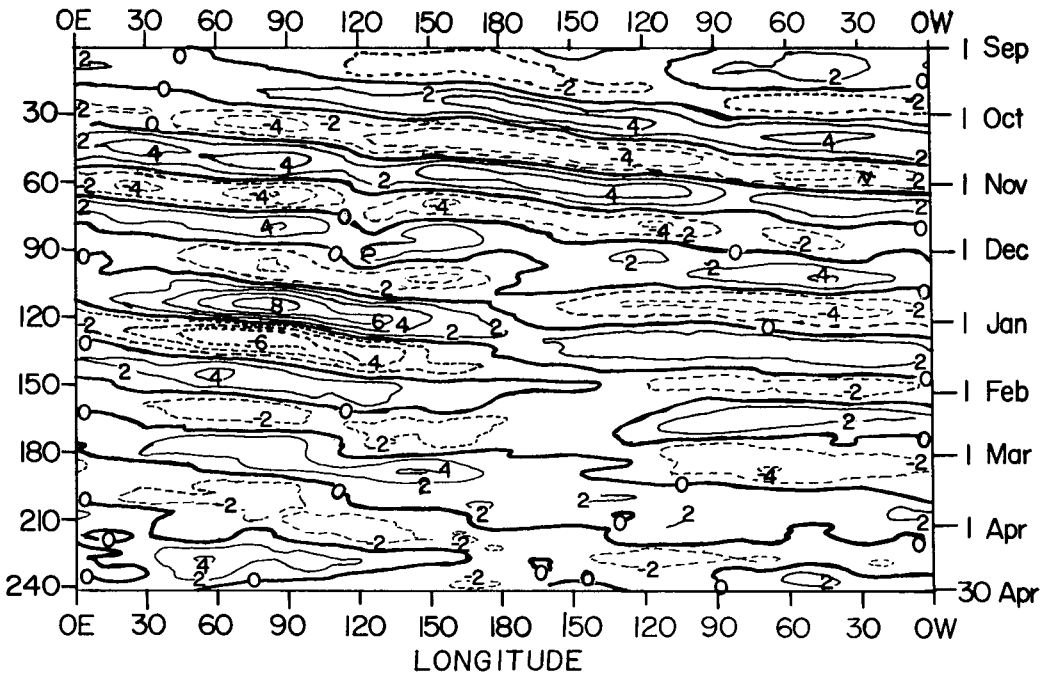

FIG. 9. As in Fig. 5, except 27–44 day filter applied to distribution of χ_2 shown in Fig. 8.

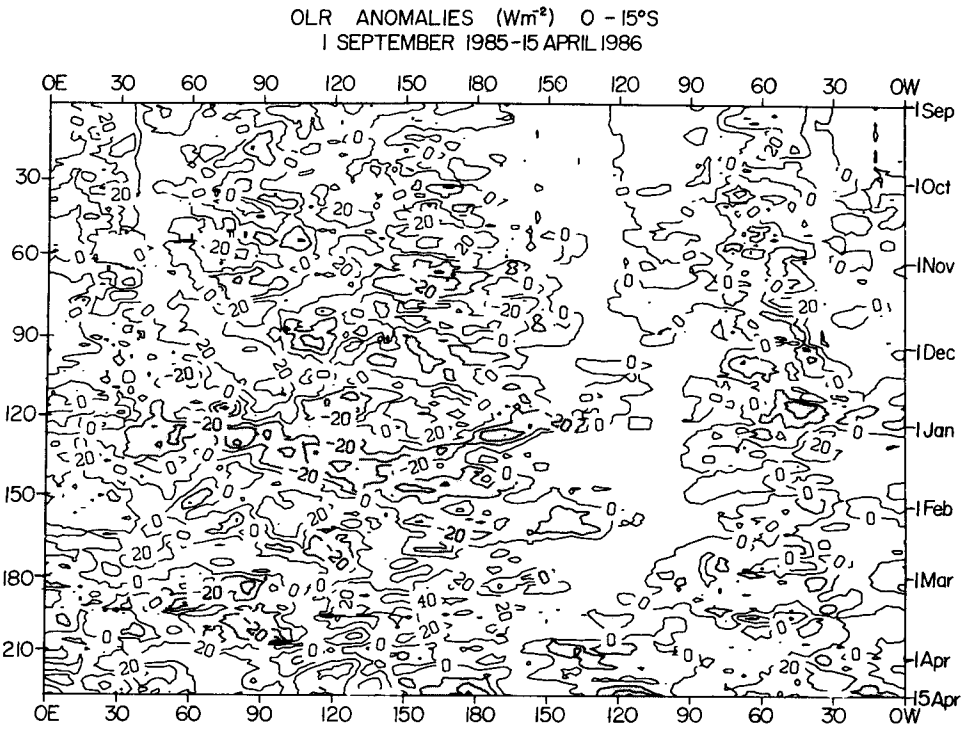

FIG. 10. As in Fig. 6, except for 1 September 1985–15 April 1986.

the 66-day period (see Fig. 7a,c,d). Because of the strong indication of the preference for a 33-day oscillation, a recursive bandpass filter was applied to the data with ω_0, ω_1, and ω_2 respectively equal to 34, 27, and 44 days. The results, which are depicted in a Hovmoeller diagram in Fig. 9, illustrate the essentially uninterrupted propagation of the 33-day wave around the globe. Furthermore, as for Year 1, it is seen that the filtered response is a substantial fraction of the total values of χ_2.

A Hovmoeller diagram of OLR is presented in Fig. 10. As for Fig. 7, the ending date of the time series is 15 April 1986. Although there is good agreement between negative anomalies of OLR (Fig. 10) and χ_2 (Fig. 8) on many occasions, there is no obvious periodicity in the OLR diagram. This is also seen in the OLR Hovmoeller diagram discussed by Weickmann (1986). Nonetheless, as was the case in Year 1, the most intense convection is seen to occur in the region stretching from the Indian Ocean to the central Pacific.

4. Summary

The purpose of the present paper was to investigate the intraseasonal oscillation of convection and related variables in the Southern Hemisphere tropics using two years of ECMWF analyses, 1 May 1984–30 April 1986. A unique aspect of the research was that the original, unfiltered, time series of several variables was first examined to find out if a statistically significant signal occurred on the intraseasonal time scale. The diagnosis showed that two variables, velocity potential at 200 hPa (χ_2) and outgoing longwave radiation (OLR), provided the best evidence of an intraseasonal oscillation. Furthermore, it showed that the oscillation was nearly nonexistent during the winter months, therefore, these data were eliminated from further consideration. Subsequently, the main part of our investigation focused on an analysis of χ_2 and OLR for two periods, 1 November 1984–30 April 1985 (Year 1) and 1 September 1985–15 April 1986 (Year 2), when both variables exhibited an important signal on the intraseasonal time scale. The major findings are now summarized.

A number of statistical tests were applied to the time series of χ_2 and OLR, with only the time mean and linear trend removed. The results for Year 1 revealed that a significant period was present from 50–67 days. The same tests applied to Year 2 yielded a significant period of approximately 33 days. Based on these results the time series of χ_2 was filtered and the recursive bandpass technique of Murakami (1979) was applied to this variable. Here 50% of the response should be retained in the 40–80 day period for Year 1 and 27–44 day period for Year 2. It is important to emphasize that the results could have been misinterpreted, and probably misrepresented, if the data had first been temporally filtered (e.g., 30–60 day bandpass), as has been the procedure of many previous investigations. Nonetheless, these findings are in agreement with those of prior studies.

When considered altogether, the analyses showed the following characteristics for the intraseasonal oscillation in the Southern Hemisphere tropics. In both years the oscillation was detectable from 60°E–180°, then it weakened as it crossed from the central to the eastern Pacific. In most cases, the χ_2-wave could be followed around the globe throughout Years 1 and 2; however, the OLR oscillation could only be detected across the Indian and western Pacific Oceans. There were some noteworthy differences between Years 1 and 2, besides the previously mentioned, statistically significant periods. The signal of the oscillation was much stronger in Year 1 than in Year 2, especially as revealed in the cross-correlation spectra of χ_2 and OLR. More specifically, the cross-correlation coefficients in Year 1 for a period of 67 days were very high from 60°E–165°W and somewhat lower from 165°–120°W, whereas in Year 2 for a period of 33 days they were generally low from 60°–120°E, higher from 120°E–180°, and lower again east of the date line. Perhaps the fact that the oscillation traveled faster in the second year is the reason for the poorer correlation then.

Acknowledgments. The authors thank Ms. Melinda Hunter for drafting the figures, Ms. Helen Henry for typing the manuscript, and Dr. James Hurrell for his programming assistance and scientific discussions with the first author. They also thank the anonymous reviewers for their helpful suggestions, which improved the manuscript, and Dr. Klaus Arpe of ECMWF for supplying the OLR data. The work was supported by: 1) the Minister of Research of the Federal Republic of Germany within the Climate Research Program under Grant 07KF2121 and 2) the National Aeronautics and Space Administration under Contract NAS8-37127 issued to Dr. D. G. Vincent, Purdue University. Much of the research was completed while Dr. Vincent was on sabbatical leave from Purdue at the Institute for Geophysics and Meteorology, University of Cologne, Germany.

REFERENCES

Gruber, A., M. Varnadore, P. A. Arkin and J. S. Winston, 1986: Monthly and seasonal mean outgoing longwave radiation and anomalies. NOAA Tech. Rep. NESDIS 26, U.S. Dept. of Commerce, NOAA/NESDIS, Washington, D.C., 20233, 7 pp. (and atlas of maps).

Gutzler, D. S., and R. A. Madden, 1989: Seasonal variations in the spatial structure of intraseasonal tropical wind fluctuations. *J. Atmos. Sci.*, **46,** 641–660.

Jenkins, G. M., and D. G. Watts, 1968: *Spectral Analysis and its Application.* Holden-Day series in time series analysis, XVIII, Holden-Day, 525 pp.

Knutson, T. R., and K. M. Weickmann, 1987: 30–60 day atmospheric oscillations: composite life cycles of convection and circulation anomalies. *Mon. Wea. Rev.*, **115,** 1407–1436.

——, —— and J. E. Kutzbach, 1986: Global-scale intraseasonal oscillations of outgoing longwave radiation and 250 mb zonal wind during Northern Hemisphere summer. *Mon. Wea. Rev.*, **114,** 605–623.

Krishnamurti, T. N., P. K. Jayakumar, J. Sheng, N. Surgi and A. Kumar, 1985: Divergent circulations on the 30 to 50 day time scale. *J. Atmos. Sci.*, **42,** 364–375.

Lau, K.-M., and P. H. Chan, 1985: Aspects of the 40–50 day oscillation during northern winter as inferred from outgoing longwave radiation. *Mon. Wea. Rev.*, **113,** 1889–1909.

Lorenc, A., 1984: The evolution of planetary-scale 200 mb divergent flow during the FGGE year. *Quart. J. Roy. Meteor. Soc.*, **110,** 427–441.

Madden, R. A., 1986: Seasonal variations of the 40–50 day oscillation in the tropics. *J. Atmos. Sci.*, **43,** 3138–3158.

——, and P. R. Julian, 1971: Detection of a 40–50 day oscillation in the zonal wind in the tropical Pacific. *J. Atmos. Sci.*, **28,** 702–708.

——, and ——, 1972: Description of global-scale circulation cells in the tropics with a 40–50 day period. *J. Atmos. Sci.*, **29,** 1109–1123.

Murakami, M., 1979: Large-scale aspects of deep convection activity over the GATE area. *Mon. Wea. Rev.*, **107,** 994–1013.

Murakami, T., T. Nakazawa and J. H. He, 1983: 40–50 day oscillations during the 1979 Northern Hemisphere summer. Tech. Rep. UHMET 83–02. Dept. of Meteor. University of Hawaii.

——, L.-X. Chen and A. Xie, 1986: Relationship among seasonal cycles, low frequency oscillations, and transient disturbances as revealed from outgoing longwave radiation data. *Mon. Wea. Rev.*, **114,** 1456–1465.

Trenberth, K. E., and J. G. Olson, 1988: ECMWF global analyses 1979–1986: circulation statistics and data evaluation. NCAR Tech. Note, NCAR/TN-300+STR, National Center for Atmospheric Research, 94 pp.

von Storch, H., T. Bruns, I. Fischer-Bruns and K. Hasselmann, 1988: Principal oscillation pattern analysis of the 30–60 day oscillation in general circulation model equatorial troposphere. *J. Geophys. Res.*, **93**(D9), 11 022–11 036.

Webster, P. J., 1983: Large-scale structure of the tropical atmosphere. *Large-Scale Dynamical Processes in the Atmosphere,* B. J. Hoskins and R. P. Pearce, Eds., Academic Press, 235–275.

Weickmann, K. M., 1985: 30–60 day atmospheric oscillation. *Climate Diagnostics Bulletin,* No. 85/4, March 1985, NOAA/NWS/NMC, Climate Analysis Center, W/NMC 52, Room 605, World Weather Building, Washington, D.C., 20233, pp. 4–5.

——, 1986: 30–60 day (intraseasonal) atmospheric oscillations. *Climate Diagnostics Bulletin,* No. 86/3, February 1985, NOAA/NWS/NMC, Climate Analysis Center, W/NMC 52, Room 605, World Weather Building, Washington, D.C., 20233, pp. 3–4.

——, G. R. Lussky and J. E. Kutzbach, 1985: Intraseasonal (30–60 day) fluctuations of outgoing longwave radiation and 250 mb streamfunction during northern winter. *Mon. Wea. Rev.*, **113,** 941–961.